JPhys Energy

PAPER • OPEN ACCESS

The effect of SO_2 on the Ni-YSZ electrode of a solid oxide electrolyzer cell operated in co-electrolysis

To cite this article: G Jeanmonod *et al* 2020 *J. Phys. Energy* **2** 034002

IOP Publishing J. Phys. Energy 2 (2020) 034002 https://doi.org/10.1088/2515-7655/ab8b55

Journal of Physics: Energy

OPEN ACCESS

RECEIVED
17 December 2019

REVISED
31 March 2020

ACCEPTED FOR PUBLICATION
20 April 2020

PUBLISHED
27 May 2020

PAPER

The effect of SO_2 on the Ni-YSZ electrode of a solid oxide electrolyzer cell operated in co-electrolysis

G Jeanmonod[1], S Diethelm[2] and J Van Herle[1]

[1] Group of Energy Materials, Swiss Federal Institute of Technology in Lausanne (EPFL), Sion 1951, Switzerland
[2] SOLIDpower SA, Avenue des Sports 26, 1400 Yverdon-les-Bains, Vaud 1001, Switzerland

E-mail: guillaume.jeanmonod@epfl.ch **and** jeanmonodg@gmail.com

Keywords: solid oxide electrolyzer, co-electrolysis, sulphur, Ni-YSZ, poisonning, low-frequency hook

Abstract

In this work, the effect of sulphur poisoning of the Ni-YSZ electrode of an SOEC operated in co-electrolysis mode was investigated. Short-term tests with exposure up to 5 ppmv of SO_2 were performed at OCV and under polarization (0.25 A cm^{-2}). The two-stages degradation pattern observed consisted of an initial fast voltage increase followed by a slower voltage increase similar to that of an SOFC exposed to H_2S. Electrochemical impedance spectroscopy and the analysis of the distribution of relaxation times showed that both the catalytic and electrochemical reactions were affected by SO_2. After extended periods in SO_2-free reactant, only a partial recovery of the performances was observed even when exposure amounted to only 0.5 ppmv of SO_2 independently on the current density. A durability test at a constant polarization of 0.5 A cm^{-2} showed a voltage 'runaway' behavior during successive exposures to 1 ppmv and 2 ppmv of SO_2. This behavior originated from a drastic increase of the serial resistance, which almost completely recovered when the SO_2 supply was cut. This behavior was not observed during exposure to 0.5 ppmv of SO_2, suggesting that, in these test conditions, the voltage 'runaway' behavior could be avoided at a sub-ppmv level. Successive exposure-recovery cycles were found to weaken the SOEC tolerance to SO_2 and a low frequency pseudo-inductive arc was observed in the impedance response during and after the second exposure to SO_2.

1. Introduction

Solid oxide electrolysis cells (SOECs) can be used to store excess renewable electricity into chemical energy by electrolysing steam [1], CO_2 [2], or a mixture of the two referred to as co-electrolysis [3]. The latter is found to be particularly interesting with downstream coupling with methane production due to the high potential for heat integration [4]. Supplying water to the SOEC is relatively straightforward due to its abundancy, whereas supplied CO_2 generally must be separated from a dilute source, such as the atmosphere (~0.04% vol CO_2) or a more concentrated one, such as flue gases (10% to 20% vol CO_2), or derived from biomass (up to 100% vol CO_2 during fermentation processes) [5]. Impurities present in the CO_2 stream used during the carbon capture process may also be present in the captured CO_2 [6]. The major impurities found in the captured CO_2 are: O_2, H_2O, N_2, NO_x, SO_x,CO, H_2, and CH_4, [6–8]. Traces of sulphur compounds may be particularly problematic for the operation of an SOEC, as solid oxide fuel cells (SOFCs) containing nickel were found to be vulnerable to sulphur compounds such as C4H4S [9], CH3SH, COS [10, 11], and H_2S [12–15].

Sulphur has been found to impact the electrochemical performance of an SOFC by reducing the catalytic reactions, such as the steam methane reforming (SMR, (1)) and the reverse water–gas shift reaction (RSWG, (2)) [16, 17], and by limiting the charge transfer processes at the triple phase boundary (TPB) [18–20].

$$CH_4 + H_2O \rightleftharpoons CO + 3H_2 \quad (1)$$

$$CO_2 + H_2 \rightleftharpoons CO + H_2O \quad (2)$$

Thermodynamic computations show that nickel sulphide (Ni_3S_2(l)) only forms at concentration of H_2S above 1%; at lower H_2S concentrations, adsorption of sulphur on nickel is prefered [14, 21]. The adsorption process can be described as:

$$H_2S(g) \rightleftharpoons S_{ad} + H_2(g), \tag{3}$$

where S_{ad} represents the sulphur adsorbed on nickel. Generally, when the sulphur supply is cut, the SOFC performance recovers partially or completely [15, 22]. Furthermore, behaviour during poisoning and recovery are dependant on the operating conditions. Generally, an increase of the operating temperature [12] or current density [15] improve the SOFC tolerance to sulphur, whereas an increase of the sulphur concentration [12, 22, 23] and the presence of CO/CO_2 as reactant compared to H_2/H_2O [24] were found to reduce the sulphur tolerance. Although H_2S is the most commonly used compound for sulphur tolerance experiments on SOFCs, [17] observed a higher rate of deactivation when a nickel catalyst was exposed to SO_2 rather than H_2S. Residual traces of SO_2 in captured CO_2 may be more critical than a similar amount of H_2S on the solid oxide cell (SOC). Therefore, operating an SOC in electrolysis rather than fuel cell mode could potentially modify the tolerance of the SOC due to the different reactant composition, the inverted polarization, and nature of the sulphur compound.

Few researcher have investigated the effects of impurities on a SOECs. Of these, Kushi [25] found that an SOC's O_2 electrode was more sensitive to SO_2 under electrolysis than under fuel cell operation. Zheng *et al* [26] investigated the effect of SO_2 on a composite lanthanum strontium cobalt manganite (LSCM) and gadolina- doped ceria (GDC) fuel-electrode during electrolysis of simulated flue gases. No significant impact on the SOEC performance was reported below 15 ppm of SO_2; electrolysis activity even improved when O_2 was also present. Ebbesen *et al* [27] were able to suppress the degradation of an SOEC, composed of a nickel yttria stabilized zirconia (Ni-YSZ) cermet reactant electrode, by cleaning the inlet gases. The degradation observed without the gas cleaning device was, thus, attributed to the presence of impurities in the inlet gases. H_2S was found in the ppb level in the supply gases (without the gas cleaning device), but the role of H_2S in the degradation was not clearly assessed.

This work therefore aims at assessing the effects of sulphur on the Ni-YSZ hydrogen electrode of an SOC performing co-electrolysis of CO_2 and H_2O. First, results obtained from short-term tests performed on SOECs with a controlled level of SO_2 at various current densities are presented. Then results of a durability test (2500 h) conducted in galvanostatic mode under exposure to SO_2 are reported. The effects of SO_2 on the performance and durability of the SOEC are evaluated using electrochemical impedance spectroscopy (EIS) and the analysis of the distribution of relaxation times (DRT).

2. Experiment description

Hydrogen-electrode (HE)-supported ceramic cells from SOLIDpower originating from the same batch were used to evaluate the impact of SO_2 on a solid oxide electrolyzer cell (SOEC). The cell is composed of a cermet Ni-YSZ HE, a YSZ electrolyte, a GDC barrier layer, and a lanthanum strontium cobalt ferrite (LSCF) oxygen electrode (OE). The cells have a diameter of 60 mm with an active area of 12.56 cm^2 (40 mm diameter). On each electrode, the gas flow is radially distributed from the centre to the border of the cell. A glass sealant is used to guarantee the gas tightness of the set up. The reduction of NiO to Ni is performed at 850 °C by slowly increasing the hydrogen content from 10% vol H_2 and 90% vol N_2 to 100% vol H_2 with a flow rate of 200 Nml min^{-1} on the hydrogen side and 500 Nml min^{-1} of air on the oxygen side.

After the reduction step, a mixture composed of 65% vol H_2O, 25% vol CO_2 and 10% vol H_2 was used on the HE side with a flow rate of 150 Nml min^{-1}. Addition of argon containing 1000 ppmv of SO_2 was used to control the concentration of sulphur dioxide in the reactant stream. The added Ar and SO_2 always represented less than 1% of the total reactant flow, the dilution effects were thus considered negligible. The OE was swept by air with a flow rate of 150 Nml min^{-1}. A gold mesh was used for current collection on the oxygen side whereas a nickel mesh was used on the hydrogen side. The tests were performed at 750 °C with a current density ranging from 0 to 0.5 A cm^{-2} and a SO_2 concentration ranging from 0.5 to 5 ppmv. The SOEC voltage was constantly monitored and its evolution was used as a first evaluation of the effect of SO_2 on the SOEC performance. Electro-chemical impedance spectroscopy (EIS) was used to identify the mechanisms involved. Measurements were taken from 20 mHz to 200 kHz with a sinusoidal perturbation of $\pm$ 200 mA (corresponding to about $\pm$ 10 to $\pm$ 15 mV). Inductance of the lead wires was limited by the use of twisted pair wires and, if necessary, high frequency points were manually removed.

When represented in a Nyquist diagram, as in figure 1, the low-frequency intercept (right hand side) of the impedance spectra represents the total cell resistance (R_{tot}), and the high frequency intercept (left hand side) the serial (or ohmic) resistance (R_s). The difference between R_{tot} and R_s gives the polarization resistance

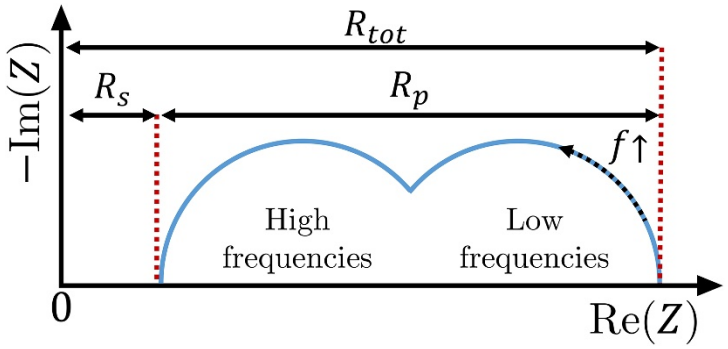

Figure 1. Schematic representation of the electrochemical impedance spectrum with the definition of the serial (R_s), polarization (R_p), and total cell resistance (R_{tot}). Z is the complex electrochemical impedance.

Table 1. Attribution of the DRT peaks to processes according to [29].

Name	Frequency	Attribution
P1	<1 Hz	Conversion and diffusion at the OE Transport in reforming mixture (HE)
P2	1 Hz to 10 Hz	Gas conversion (HE)
P3	10 Hz to Hz to 100 Hz	HE diffusion OE reaction and solid state diffusion
P4	100 Hz to 500 Hz	Secondary peaks (HE and OE transport)
P5	0.5 Hz to 100 Hz	HE charge transfer
P6	5 Hz to 200 Hz	Not attributed[a]

[a]Possibly: solid–solid OE transfer processes or electronic current losses between the OE and the current collector

(R_p). R_s and R_p are used to identify and quantify the degradation processes. To get a better insight into the degradation process, the distribution of relaxation times (DRT), γ, of selected electro-chemical impedance spectra was computed using Tikonov regularization [28]. For consistency with the Nyquist representation of the impedance spectra used in this work, the DRT is represented in terms of frequency rather than time. The attribution of the DRT peaks to processes are made according to [29], who performed an extensive experimental sensitivity analysis combined with a dynamic numerical model on SOCs originating from the same provider. Six DRT peaks were identified and are presented in table 1.

3. Results and Discussion

Thermodynamic equilibrium calculations performed with HSC Chemistry 8.2.0 [30] showed that, with the reactant gas mixture used, SO_2 is not stable at 750 °C under 1 atm and tends to form H_2S. However, the kinetics of the decomposition reactions was not considered in this computation. The exact chemical form of the sulphur compound present at the hydrogen electrode is, thus, not exactly known. The thermodynamic equilibrium gas composition at 750 °C is 67.2% vol H_2O, 22.9% vol CO_2, 7.9% vol H_2, and 2.1% vol CO, which differs from the sent reactant gas mixture due to the RWGS reaction.

3.1. The effect of polarization and SO_2 concentration

3.1.1. Open circuit conditions

An SOEC, under open-circuit conditions, was exposed to 0.5, 1, 2 and 5 ppmv of SO_2 during a period ranging from 19 to 24h intercalated with a 20 h recovery period during which the cell was flushed with an SO_2-free reactant. Before the first exposure to SO_2, the measured cell voltage (V_0) was only 2 mV above the theoretical Nernst potential computed using the reactant composition at thermodynamic equilibrium, 0.865 and 0.863V, respectively. This indicated that the reactant flow was close to the thermodynamic equilibrium and that the SOEC sealing was gas-tight.

When exposed to SO_2, the SOEC voltage showed a step-like increase pattern, as presented in figure 2(a). The height of the step, computed from V_0, and the slope of the step appeared to be correlated with the SO_2 concentration as presented in table 2. After this initial step increase, the voltage steadily increased at a rate of about 20 to 30 mV kh^{-1}, without any apparent relation with the SO_2 concentration. A schematic representation of the SOEC's voltage evolution during SO_2 poisoning defining the values reported in table 2

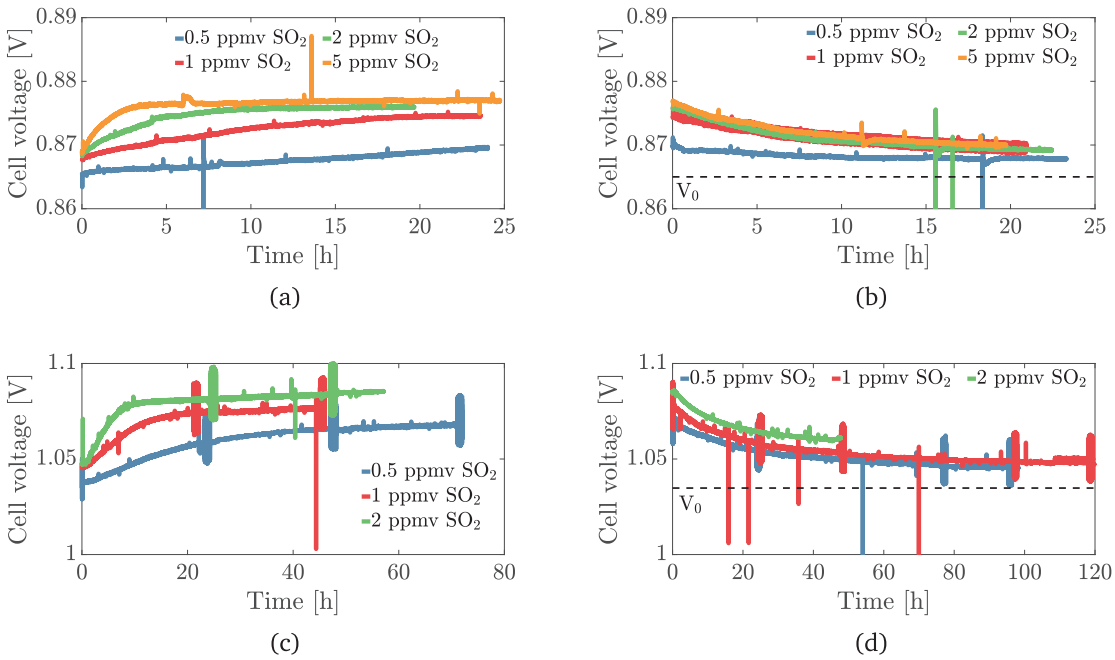

Figure 2. Time evolution of the cell voltage when exposed to various concentrations of SO_2 and during recovery at OCV (a) and (b), respectively, and at 0.25 A cm^{-2} (c) and (d), respectively .

is presented in appendix A. When the exposure to SO_2 was stopped, the voltage almost instantaneously started decreasing. The recovery was much slower than the contamination and was never complete, suggesting an irreversible effect of sulphur even after exposure to only 0.5 ppmv of SO_2. The rapid initial degradation followed by a reduced and constant deactivation and a slower recovery process once the sulphur supply was stopped was in good agreement with observations reported for solid oxide fuel cells exposed to sulphur compounds [9, 14, 18, 23, 24]. As the SOEC was not polarized, it was similar as testing an SOFC at high H_2O and CO_2 content. The initial voltage step was thus attributed to the same process than for an SOFC: adsorption of sulphur on nickel, reducing both the catalytic and electrochemical performances of the SOEC. Analogously to (3), this adsorption reaction can be described as

$$H_2S(g) \rightleftharpoons S_{ad} + H_2(g) \tag{4}$$

or

$$SO_2(g) \rightleftharpoons S_{ad} + O_2(g), \tag{5}$$

depending whether sulphur is present in the form of H_2S or SO_2, where S_{ad} represents the sulphur adsorbed on Ni.

As no bias current was applied, solely a modification of the gas composition at the hydrogen electrode would affect the measured cell voltage. It was thus assumed that the catalytic reactions (i.e. RWGS reaction) were limited due to the coverage of nickel by sulphur preventing the feed gas to reach the thermodynamic equilibrium composition. This is in agreement with Hagen [24] and He *et al* [31], who reported a deactivation of the RWGS reaction when the nickel-based anode of an SOFC operating on syngas was exposed to H_2S.

The deviation from the thermodynamic equilibrium was then evaluated by assuming that the measured open circuit voltage (OCV) corresponded to the Nernst potential of an effective gas composition between the inlet and thermodynamic equilibrium composition. Using HSC Chemistry 8.2.0 [30], thermodynamic equilibrium gas compositions were computed at varying effective temperatures until the corresponding Nernst potential matched the measured OCV. The difference between the effective and actual operating temperature is then representative of the deviation of the composition from the thermodynamic equilibrium. The observed increase in OCV due to the presence of SO_2 thus corresponds to a thermodynamic equilibrium composition at an effective temperature lower than the actual operating temperature, indicating a reduction of the RWGS reaction. The increase of 12 mV observed after exposure to 5 ppmv of SO_2 seen in figure 2(b) corresponded to a 25 °C decrease of the effective temperature. As the CO

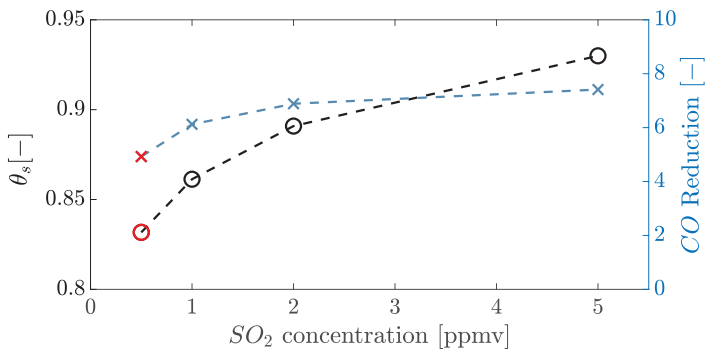

Figure 3. Ni coverage and reduction of the CO content with respect to the SO_2 content. The reduction of the CO content was computed based on the equivalent composition corresponding to the initial OCV measured. The red data points are extrapolated data.

Table 2. Height of initial degradation step measured from the initial and recovered (in between parentheses) voltage, the initial degradation rate, and the final degradation rate, as defined in appendix A, when the SOECs were polarized at a current density *j* and exposed to various concentrations of SO_2.

j A cm^{-2}	SO_2 ppmv	Initial degradation step height mV	Initial degradation step rate mV kh^{-1}	Final degradation rate mV kh^{-1}	Time to stabilization h
0	0.5	8[a]	200	not stabilized	40[a]
	1	9 (7)	400	20	20
	2	11 (7)	1100	30	10
	5	11 (8)	2500	20	4
0.25	0.5	28	1000	100	40
	1	36 (28)	2300	100	20
	2	42 (33)	4600	100	10
0.5[b]	1	14	26'500	60	7.7
	1	24 (12)	29'500	40	5.3
	2	28 (15)	100'300	100	3.3
	0.5	27 (14)	11'400	30	20

[a]Linearly extrapolated based on the stabilization times obtained with other SO_2 concentration and the initial degradation slope
[b]These results, obtained during the durability test, are discussed in the section 3.2

content of the equilibrium reactant composition originated only from the RWGS reaction, its variation relative to the composition before exposure to SO_2 was used as a quantitative indicator of the modification of the catalytic activity. In figure 3, reduction of the CO content is compared with the surface coverage of Ni using the correlation (6) proposed by Hansen [32] that was originally developed for H_2S and adapted here by simply replacing the partial pressure of H_2S by the partial pressure of SO_2. Further work is needed to assess the validity of this adaptation for SO_2.

$$\theta_s = 1.45 - 9.53 \cdot 10^{-5} \cdot T + 4.17 \cdot 10^{-5} \cdot T \cdot \ln \frac{p\mathrm{SO}_2}{p\mathrm{H}_2} \tag{6}$$

When the cell was exposed to 5 ppmv of SO_2, the surface coverage reached 0.93, whereas the CO content decreased by only 7.5%. Also, the reduction of the CO content seemed to stabilize below 10%. The effect of SO_2 on the RWGS reaction was thus relatively small, thanks to the high nickel content present in the HE (acting as a catalyst and electro-catalyst), and the nickel current collector (acting as a catalyst). However, the reduction of the catalytic activity in the vicinity of the TPB may still have significant impact on the SOEC performance under polarization due to the limited RWGS reaction reducing the local steam content.

The modification of the electro-chemical performances of the SOEC was assessed by performing EIS measurements after each exposure to SO_2 and after each recovery period. The results, summarized in figure 5, showed that the major degradation occurred between 10 Hz and 10 kHz, whereas no increase of R_s was observed. The DRT results (figure 5(c)) showed clearly that the major contribution to the increase of R_p occurred on the peak located around 1 kHz, which is associated with the charge transfer processes occurring at the HE. The peak increased drastically and shifted towards a lower frequency, leading to the covering of the peak located around 100 Hz, which is related to the transport processes in the hydrogen and oxygen

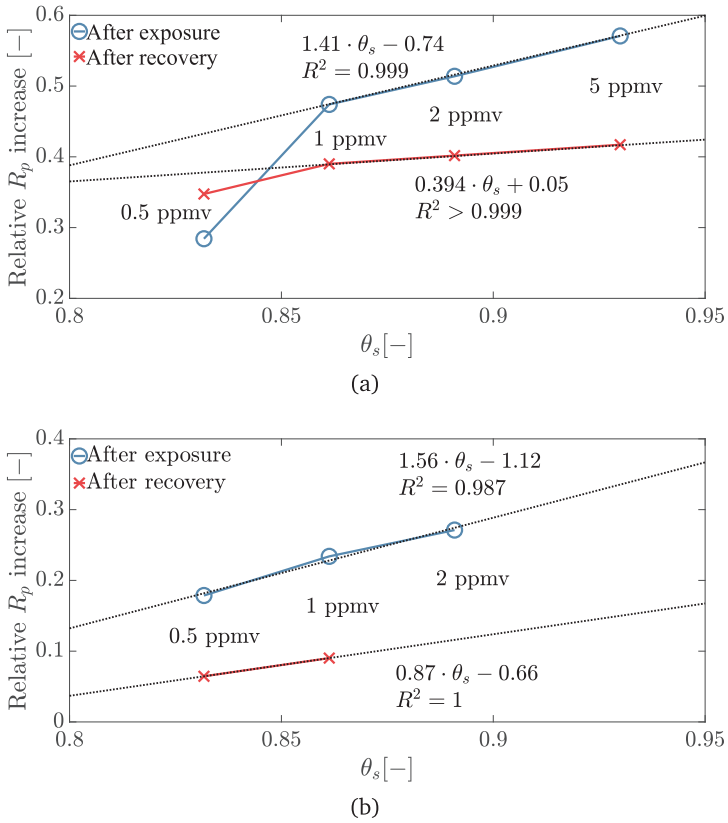

Figure 4. Relative increase of R_p after exposure to SO_2 and after recovery in function of the surface coverage at a current density of (a) 0 A cm^{-2} and (b) 0.25 A cm^{-2}.

electrode, making the deconvolution impossible. Even though the measured cell potential mostly recovered from the exposure to SO_2, the impedance response did not completely recover, suggesting that part of the Ni active sites remained covered. During the recovery following the exposure to 0.5 ppmv of SO_2, the DRT peak located around 1 kHz kept increasing, despite the decreasing (i.e. recovering) OCV. The current collector, being made of Ni, likely adsorbed sulphur during the exposure period and then slowly released it during the recovery period, thus acting as a sulphur buffer. This may have provided enough time and supply for sulphur to deposit on the active Ni, leading to the observed increase of impedance even after the SO_2 supply was shut off.

The increase of R_p after exposure to SO_2, presented in figure 4, showed a linear dependency with the Ni surface coverage, similarly to the results reported by Hansen [32] for H_2S poisoning. The polarization resistance obtained after exposure to 0.5 ppmv SO_2 was not considered here as it did not reach a stable state. The multiplicative coefficient of the linear interpolation was in good agreement with the results reported by Madi *et al* [9] for an SOFC operated on synthetic bio-gas containing various amounts of thiophene. To a smaller extent, the increase of R_p after recovery was also found to be linearly dependent on θ_s indicating that the retentive effect of SO_2 exposure was likely related to permanently adsorbed sulphur.

3.1.2. Under polarization (0.25 A cm^{-2}*)*

A second SOEC was exposed to 1 ppmv of SO_2 during 25 h followed by a 40 h recovery period. The cell was, then, polarized at 0.25 A cm^{-2} and successively exposed to 0.5, 1, 2 ppmv of SO_2 during a period ranging from 45 to 70 h each time followed by a recovery period where the cell was flushed with a SO_2-free reactant.

Under polarization, the SOEC showed a step-like degradation when exposed to SO_2, as shown in figure 2(c), similarly to the OCV case. The initial degradation step height was about two to three times larger when the cell was polarized compared with the OCV case but the time needed to reach a stabilized state was similar regardless of whether a 0.25 A cm^{-2} bias was applied or not as seen in table 2. However, the final degradation rate was about three to four times higher under polarization than at OCV. When the exposure to SO_2 was stopped, the SOEC voltage decreased in a parabolic manner but the recovery was never complete, as presented in figure 2(d). During the recovery process, after exposure to 2 ppmv of SO_2, a technical issue with the galvanostat ended the test prematurely, thus only EIS data after exposure to 0.5 and 1 ppmv were available.

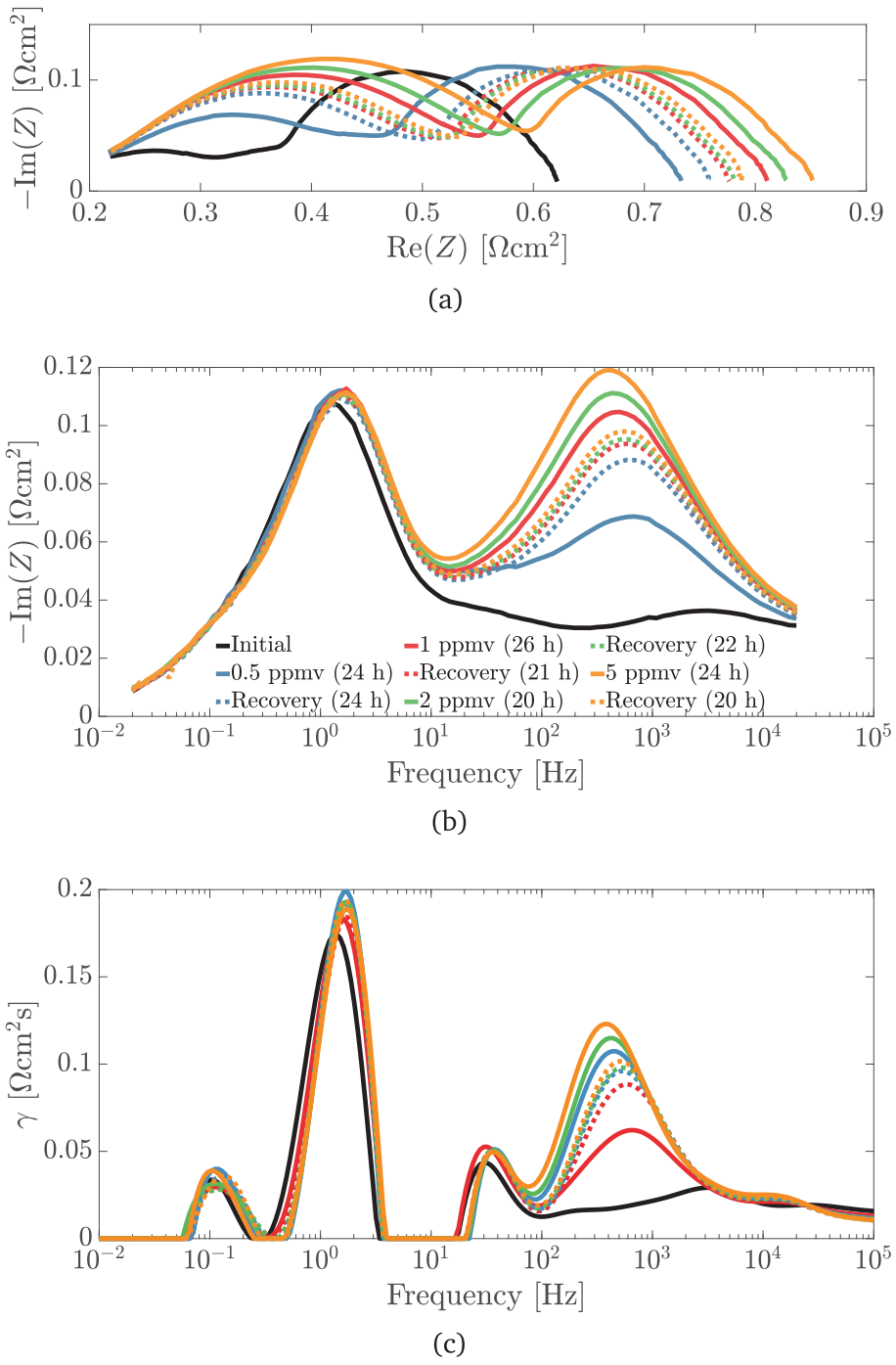

Figure 5. (a) and (b) electrochemical impedance spectra taken at OCV after exposure to 0.5, 1, 2, 5 ppmv of SO_2 followed by a recovery period without SO_2 and (c) corresponding distribution of relaxation time. The exposure/recovery durations are indicated in parentheses.

EIS measurements taken after 72 h of exposure to 0.5 ppmv of SO_2 showed that both the high and low frequency processes were affected, as shown in figure 6(a) and (b). Analysis of the DRT results of the impedance spectra showed that the peaks located around 1 Hz and between 100 Hz and 1 kHz increased, as presented in figure 6(c). The peak located around 1 Hz is sensitive to the reactant composition [29], which was coherent with a reduction of the catalytic reactions due to the coverage of nickel by sulphur [24]. This degradation should eventually stabilize when the equilibrium between the surface coverage and the sulphur content in the reactant is reached. The increase of the peak located around 1 kHz was indicative of a deterioration of the charge transfer processes and a modification of the gas composition. The behavior observed for an SOEC operated in co-electrolysis mode was found to be very similar to the one reported for

an SOFC operated under reformate operation [19, 20] indicating an analogous contamination process independently of the current direction.

Increasing the SO_2 content to 1 ppmv led to an increase between 100 Hz and 1 kHz; no significant changes were observed around 1 Hz, suggesting that a saturation was reached (figure 6). When the SO_2 content was raised to 2 ppmv, no further significant changes were observed when compared with 1 ppmv (figure 6). After the recovery period, the peak located around 1 kHz shifted back to its original relaxation frequency but did not recover completely, whereas the peak located around 1 Hz almost completely recovered.

Similarly to the OCV tests, the relative increase in R_p showed a linear behavior with respect to θ_s as presented in figure 4(b). The relative increase in R_p was found to be smaller than at OCV but this was likely due to the test history. The initial impedance response at 0.25 A cm^{-2} (figure 4) was not measured on a 'fresh' SOEC but after exposure at OCV to 1 ppmv of SO_2 and a recovery period. The relative increase of R_p was, thus, not computed on the same basis and can not be directly compared. The coefficients multiplying θ_s in figures 4(a) and (b) represents the sensitivity of the relative increase in R_p towards θ_s. This coefficient was larger when the SOEC was polarized compared to the OCV case, 1.56 and 1.41 respectively, indicating that the SOEC was more sensitive to an increase of the SO_2 content when polarized. It suggested that the polarization had a negative impact on the SOEC tolerance to SO_2.

Under polarization, hydrogen was generated, which should reduce the surface coverage of nickel by sulphur, according to correlation (6). However, due to the logarithmic dependency on the hydrogen partial pressure and the low reactant utilization (0.15 at 0.25 A cm^{-2}), this effect was likely negligible. In SOFC operation, the current density was found to improve the sulphur tolerance [15, 33, 34]. It was suggested that a higher oxygen ion flux at the triple phase boundary could help the desorption of the adsorbed sulphur by oxidation, which can be expressed as the reverse of (5). During operation as an SOEC, the opposite effect could be expected, as the polarity and thus oxygen ion flux is inverted. However, prior researchers have shown no [35] or a negative impact [36, 37] of the current density on the sulphur tolerance of an SOFC. Further investigation should, thus, be performed to clearly assess the effect of current density on the sulphur tolerance of an SOEC.

3.2. The effect on durability

Another SOEC was operated during 2500 h at 0.5 A cm^{-2} with periodic exposure to SO_2 to assess the long-term stability; the time evolution of the cell voltage and SO_2 concentrations are presented in figure 7. In the first 200 h, the SOEC showed the same step-like degradation pattern as presented before, i.e. a fast degradation (0–15 h) followed by a reduced and constant degradation (15–200 h). When compared with exposure to 1 ppmv of SO_2 at lower current density, the initial degradation rate and the time to stabilization were strongly affected by the current density, whereas no apparent link was found with the height of the initial degradation step and the final degradation rate. At 0.5 A cm^{-2}, the kinetics of sulphur adsorption on nickel was likely promoted more than at a lower current density.

In the first 11 h, the degradation was only caused by an increase of R_p, as shown in figure 8, where the time evolution of R_s and R_p is represented. According to the DRT of the EIS measurements taken during the rapid degradation, shown in figure 9, the high-frequency impedance increased first, followed by an increase over the entire spectrum until a relative stabilization. The DRT peak located around 1 kHz increased massively and shifted towards a lower frequency, which is likely due to the adsorption of sulphur on the nickel active-sites affecting the electrochemical conversion of H_2O/H_2 and CO_2/CO [19, 20]. The DRT peak located around 1 Hz first decreased and widened, and then increased while shifting towards a higher frequency. The width of a DRT peak can be related to the spatial distribution of the relaxation time associated to a particular phenomenon [38], e.g. due to inhomogeneities in the micro-structure [39]. During the initial fast degradation caused by sulphur, Rasmussen and Hagen [18], and Hagen [24] observed a peak of the in-plane voltage that was attributed to a redistribution by the current due to the progressive adsorption of sulphur on nickel from the inlet to the outlet. The widening of the DRT peak located around 1 Hz was thus assumed to be the result of the progressive adsorption of sulphur on nickel, which locally reduced the catalytic and electrochemical reactions modifying the reactant composition until the nickel coverage was at equilibrium. The peak located around 25 Hz increased and shifted towards higher frequency, suggesting that the diffusion processes at the HE were impacted. As a consequence of the various peak shifting, the DRT between 10 Hz and about 30 kHz was compressed in a smaller frequency range after the exposure to SO_2, making the deconvolution of the different processes involved more complicated.

After the initial fast voltage rise, the degradation rate was constant at about 60 mV kh^{-1} until 200 h, where both R_p and R_s started rising, as shown in figure 8. The degradation rate then increased to 200 mV kh^{-1}. After about 400 h, the voltage started rising exponentially due to an increase of R_s, whereas R_p remained almost constant, thus suggesting the presence of a cumulative effect due to the exposure to SO_2.

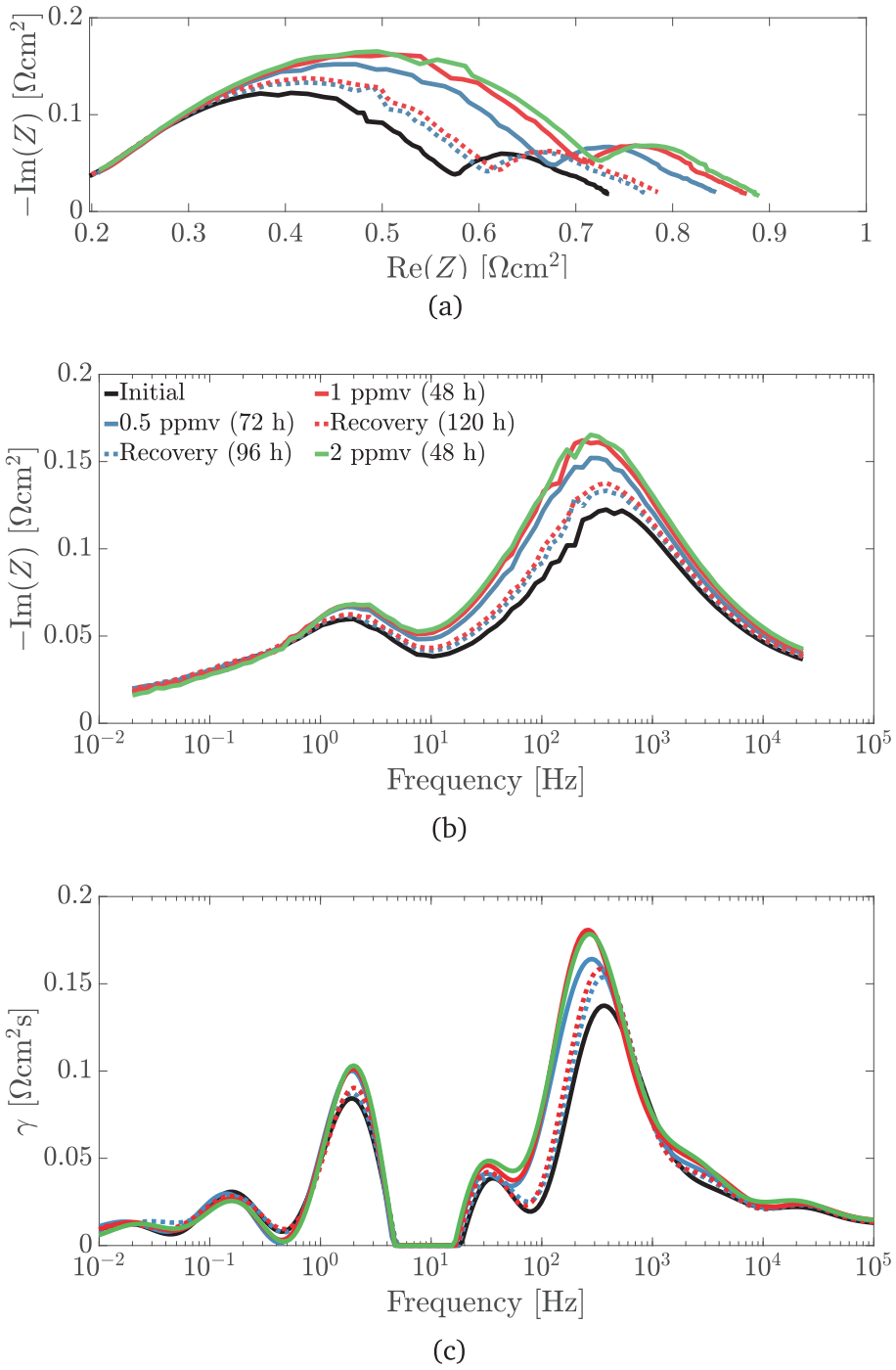

Figure 6. (a) and (b) electrochemical impedance spectra taken at 0.25A cm^{-2} after exposure to 0.5, 1, 2 ppmv of SO_2 followed by a recovery period without SO_2 and (c) corresponding DRT. The exposure/recovery durations are indicated in parentheses.

After 485 h, the exposure to SO_2 was stopped to limit the voltage increase. After less than 5 h, likely due to the presence of residual SO_2, R_p and R_s started decreasing simultaneously. After about 280 h of recovery, only R_s and the low-frequency region of the EIS had partially recovered, whereas the high-frequency region of the EIS (charge transfer) remained almost unchanged, as shown in figure 10(a) and (b).

Analysis of the DRT of the impedance spectra, presented in figure 10(c), showed that when the SO_2 supply was shut off, the conversion peak (around 1 Hz) greatly recovered but was still shifted to higher frequency, whereas the low-frequency peak (around 0.1 Hz) widened and shifted towards higher frequency. The charge transfer peak (around 1 kHz) continued increasing while shifting towards higher frequency and getting sharper. The electrochemically active sites were, seemingly affected more permanently by sulphur compared with the rest of the cell, also suggesting, a negative impact of the current density on the SOEC

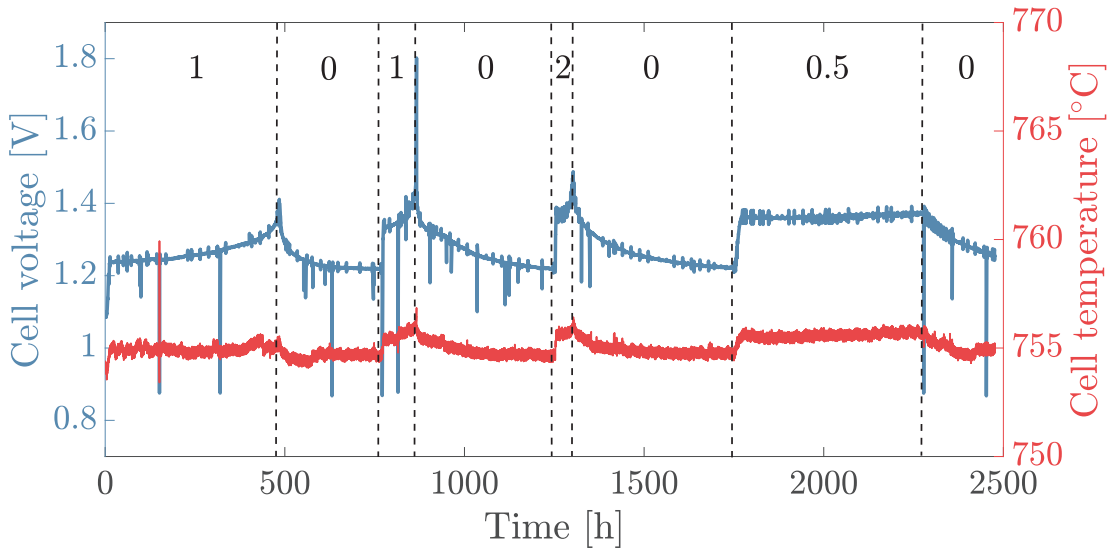

Figure 7. Time evolution of the cell voltage and temperature during the long-term stability test, where the number at the top indicates the SO_2 concentration in ppmv.

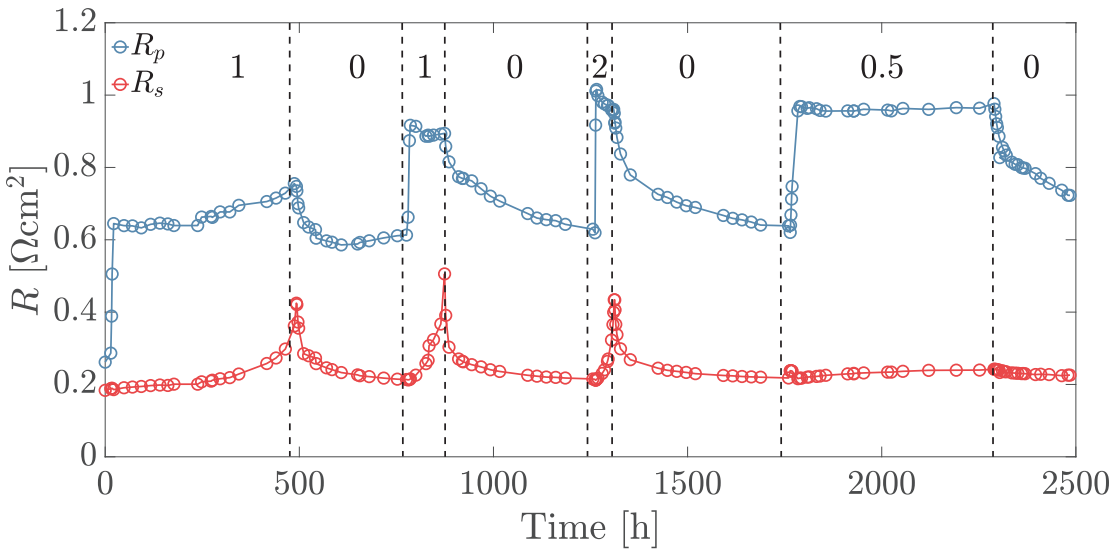

Figure 8. Time evolution of R_s and R_p during the long-term stability test, where the number at the top indicates the SO_2 concentration in ppmv.

durability when exposed to SO_2. During the recovery process, the shape of the low-frequency region of the impedance spectra changed noticeably, especially below 0.1 Hz (figure 10(b)), which resulted in the presence of a new peak at very low frequency (around 30 mHz), as shown in figure 10(c). The DRT fingerprints between 10 Hz and about 30 kHz remained compressed to a smaller frequency range.

The SOEC was then exposed to 1, 2, 0.5 ppmv intercalated with a recovery period; the resulting SOEC voltage and cell temperature evolution are reported in figure 7. A similar behavior to the first exposure was observed: a fast initial increase of the cell voltage in the first hours after the introduction of SO_2 followed by a slower voltage increase, which eventually started to run away due to a drastic increase of R_s (only when exposed to 1, and 2 ppmv of SO_2), as shown in figure 8. The height of the initial step-like degradation was not found to be dependent on the SO_2 concentration, whereas the initial degradation rate and the time to stabilization appeared linked to the SO_2 concentration, as presented in table 2.

3.2.1. Voltage 'runaway'

The drastic increase of R_s occurred earlier when the SOEC was exposed to 1 ppmv of SO_2 for the second time and even earlier under 2 ppmv of SO_2. The polarization resistance between about 30 Hz and 1 kHz was the

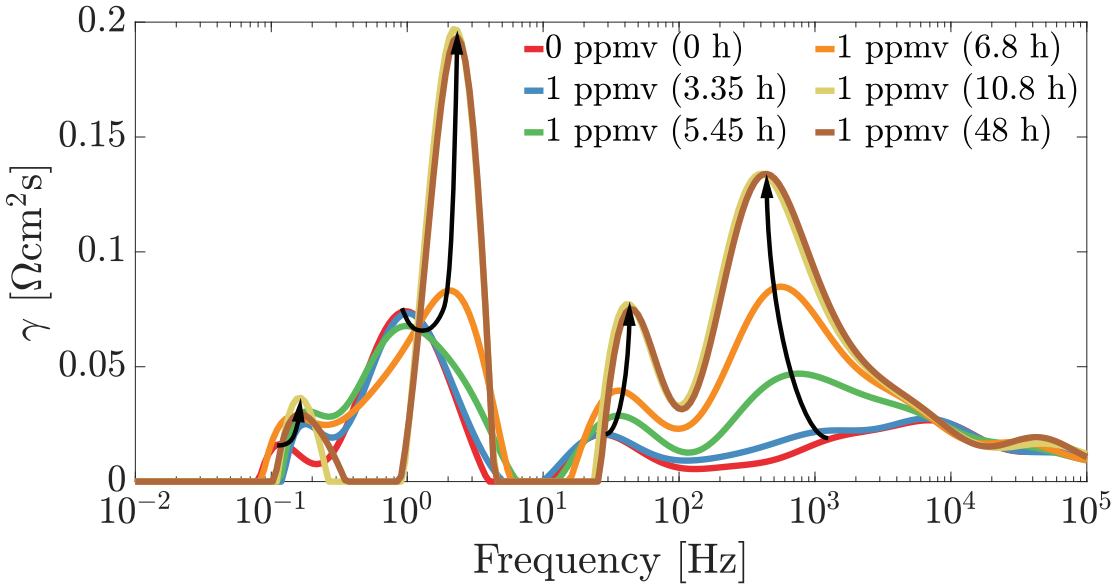

Figure 9. Time evolution of the DRT during the long term stability test, where the arrows represent the observed trends.

highest during the last exposure, even though the SO_2 concentration was the lowest (0.5 ppmv). It indicated the presence of a cumulative effect caused by the successive exposure–recovery cycles.

The time needed to reach the voltage 'runaway' regime was shorter during the second exposure to 1 ppmv of SO_2, suggesting a weakening of the SOEC after the first exposure. The voltage 'runaway' regime was reached even more quickly during the exposure to 2 ppmv of SO_2. When the SO_2 supply was cut, R_s and R_p again decreased, confirming that the 'runaway' behavior observed was linked to the presence of SO_2 in the reactant. When the SOEC was exposed to 0.5 ppmv of SO_2, however, the initial voltage increase was also present, but the voltage 'runaway' was not observed even after more than 500 h of exposure. The 'runaway' behavior thus appeared to be dependent on the history of exposure to SO_2 and only occurred above a certain SO_2 concentration.

When an increase in serial resistance was reported for an SOFC exposed to H_2S, it was found to be irreversible [40, 41], suggesting a different degradation and/or recovery mechanism for an SOEC exposed to SO_2. Two possible mechanisms, discussed in more detail in appendix B, are proposed to explain the reversible increase of R_s:

- A progressive reduction of the active area due to the deactivation by sulphur of the electrochemically active Ni from the higher (inlet) to lower (outlet) current density regions. Assuming an analoguous behavior to an electrode partial delamination, a comparable increase of R_s and R_p would be expected [42]. This is thus unlikely to be solely responsible for the observed behavior.
- A cumulative effect of sulphur blocking the electrochemically active regions located closest to the electrolyte, possibly from the higher (inlet) to lower (outlet) current density regions. The thickness of the electrolyte being on the order of 10 μm, the extent of the deactivated region would be in the order of 2 μm, considering that R_s increased by a factor of 2 to 3.

3.2.2. Low-frequency hook

During the second exposure to 1 ppmv of SO_2, a pseudo-inductive behavior began to appear at low frequency when the SOEC was exposed to sulphur and during part of the recovery, as shown in figure 11. This low-frequency pseudo-inductive behavior appeared to be more intense at the beginning of the exposures and then lowered in intensity, but did not completely disappear. It then slowly disappeared during the recovery period, as shown in figure 12(a) after exposure to 0.5 ppmv of SO_2. Figure 12(b) shows that during the recovery, the low-frequency hook seemed to transit from an pseudo-inductive to a capacitive behavior only after the region around 2 Hz mostly recovered.

Analysis of the DRT of the impedance measurements (figure 12(c)) indicated that the peak located around 1 kHz first increased and then decreased while shifting towards higher frequency during the entire recovery period, whereas the peak located around 100 Hz appeared to continuously improve and shift slightly towards a higher frequency. Due to the major overlapping of the DRT peaks between about 30 Hz and 1 kHz (figure 12(c)), the observed peak transformation could originate from the peak itself or the interaction with a

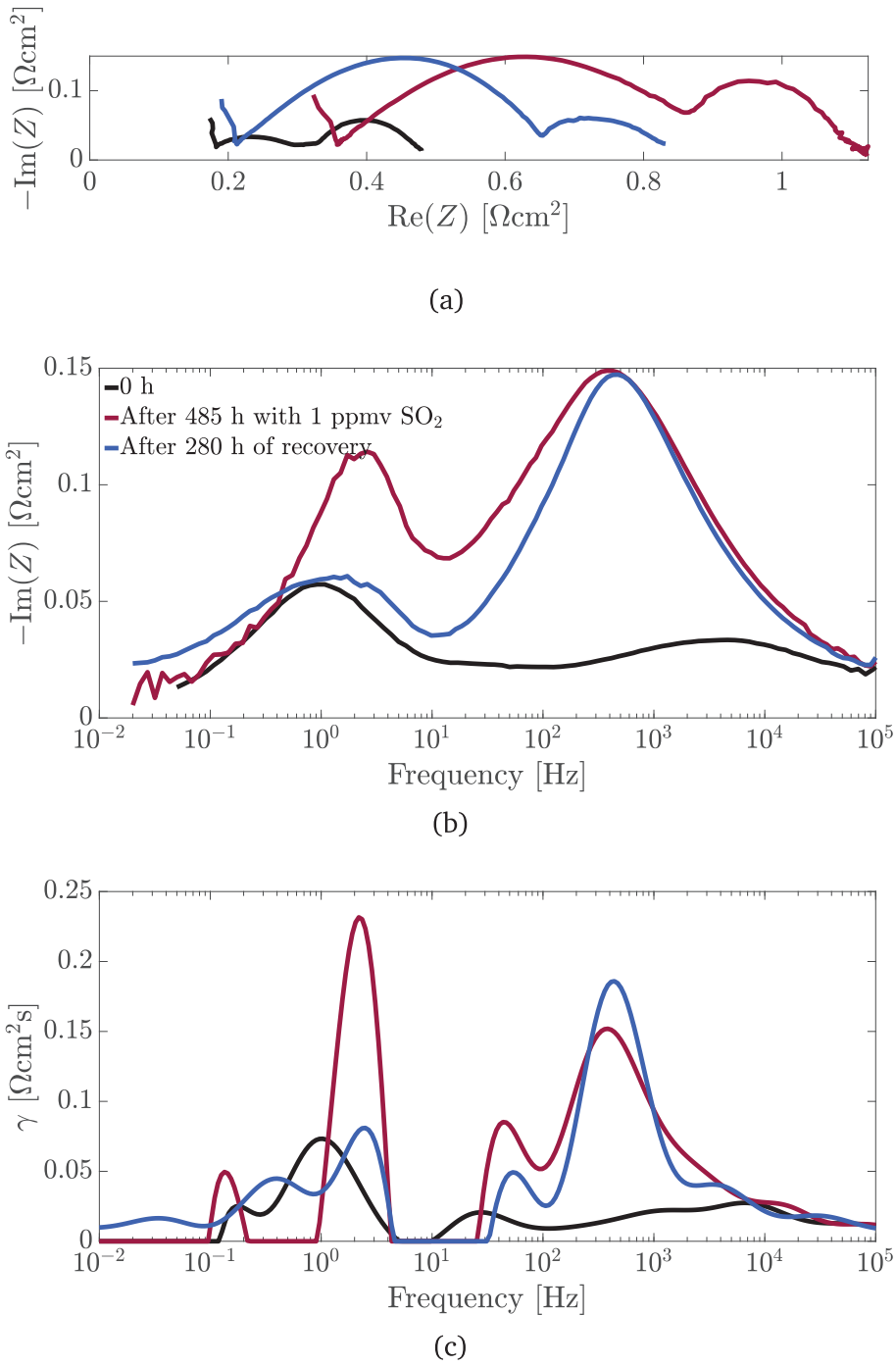

Figure 10. (a) and (b) electrochemical impedance spectra taken at 0.5 A cm^{-2} during the first exposure to 1 ppmv of SO_2 followed by a recovery period without SO_2 and (c) corresponding DRT.

neighbouring peak, making the physical interpretation complex. The other recovery periods showed a similar behavior except after the first exposure to SO_2. The low-frequency hook was not present during the first exposure period and was more intense when the cell was exposed to 2 ppmv of SO_2 than 1 ppmv (second exposure) but less than when exposed to 0.5 ppmv, as shown in figure 11. This suggests that the inductive hook originated from the exposure–recovery cycling rather than from the concentration of SO_2 itself.

After the recovery period subsequent to the exposure to 0.5 ppmv of SO_2, EIS measurements were performed in co-electrolysis (65% H_2O, 25% CO_2, 10% H_2) and steam-electrolysis (90% H_2O, 10% H_2) mode. Both showed an inductive hook at 0.75 A cm^{-2} but not at 0.5 A cm^{-2}, indicating that the presence of CO_2 was not or only partially responsible for the low-frequency hook, whereas the current density or the overpotential plays a key role.

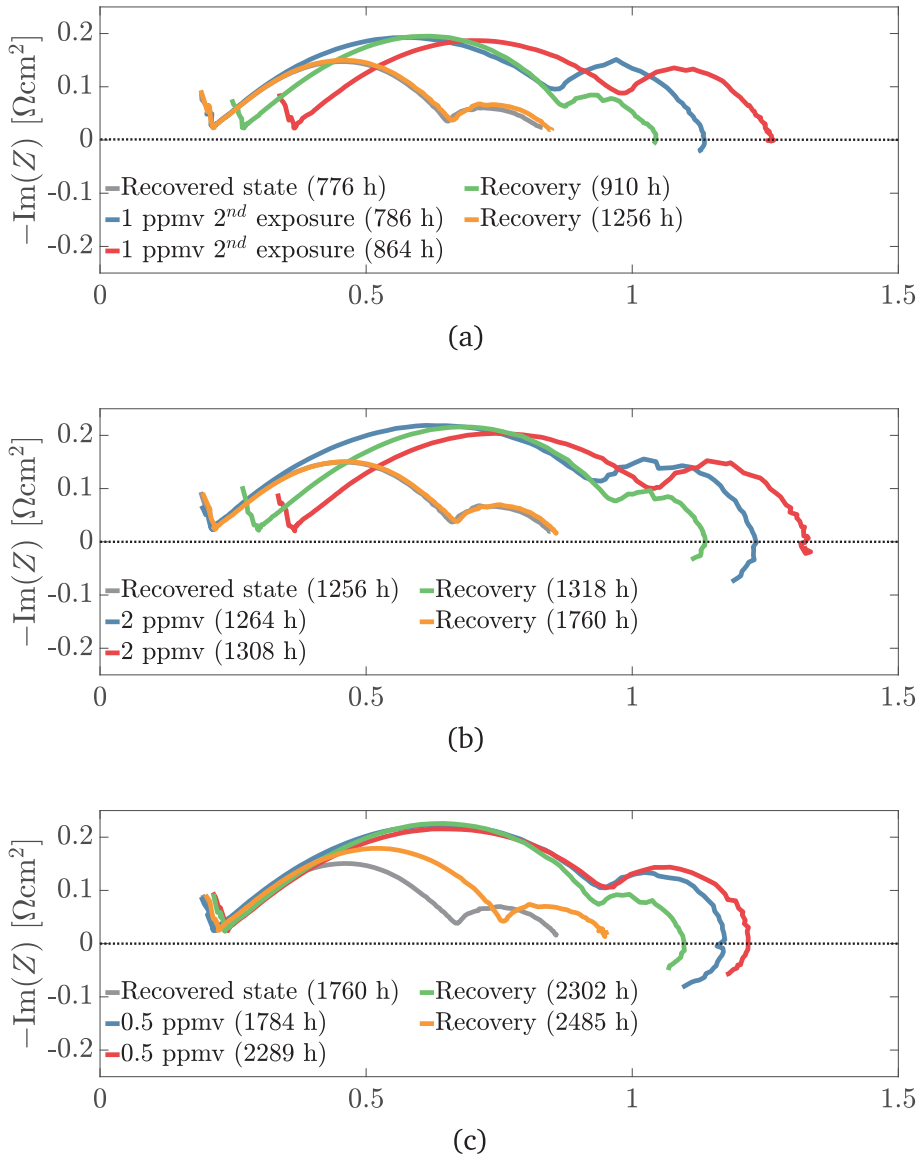

Figure 11. Electrochemical impedance spectra taken at 0.5 A cm^{-2} during the exposure to (a) 1 ppmv, (b) 2 ppmv, and (c) 0.5 ppmv of SO_2 followed by a recovery period without SO_2. The time from the beginning of the test at which the impedance spectra were measured is indicated in between parentheses.

The low-frequency hook may be caused by a two-step reaction that involves an intermediate [43–45]. Nechache *et al* [46] observed a low-frequency hook in the impedance spectra of an SOEC operated in steam-electrolysis and attributed it to the deposition of Si-containing impurities (originating from the glass gas sealing) in the HE that limited the electrochemical reduction and transport of H_2O. They concluded that when a sufficiently high current density is applied, an additional reaction mechanism, with a characteristic frequency between 1 and 10 mHz and involving adsorption of H_2O, counterbalances the negative effects of Si-containing deposits. In electrolysis operation, the electronic conductivity of the YSZ electrolyte was also found to induce a low-frequency inductive arc [47]. Due to the clear correlation with the exposure to SO_2, it was assumed that the low-frequency hook originated from the HE but was not related to the deposition of Si-containing impurities. The low-frequency hook observed could then originate from either the activation of an additional reaction mechanism involving an intermediate [46] or electronic conductivity of the YSZ [47], compensating for the deactivation of electrochemical active sites by sulphur. The presence of a low-frequency hook after recovery can be explained by the presence of residual sulphur on electrochemical active sites. A higher current was then necessary to activate the additional reaction mechanism.

4. Conclusions

The effect of SO_2 in the reactant gas stream of an SOE, with an Ni-YSZ hydrogen electrode operated in co-electrolysis was investigated. Independently of the current density, exposure to as little as 0.5 ppmv of SO_2

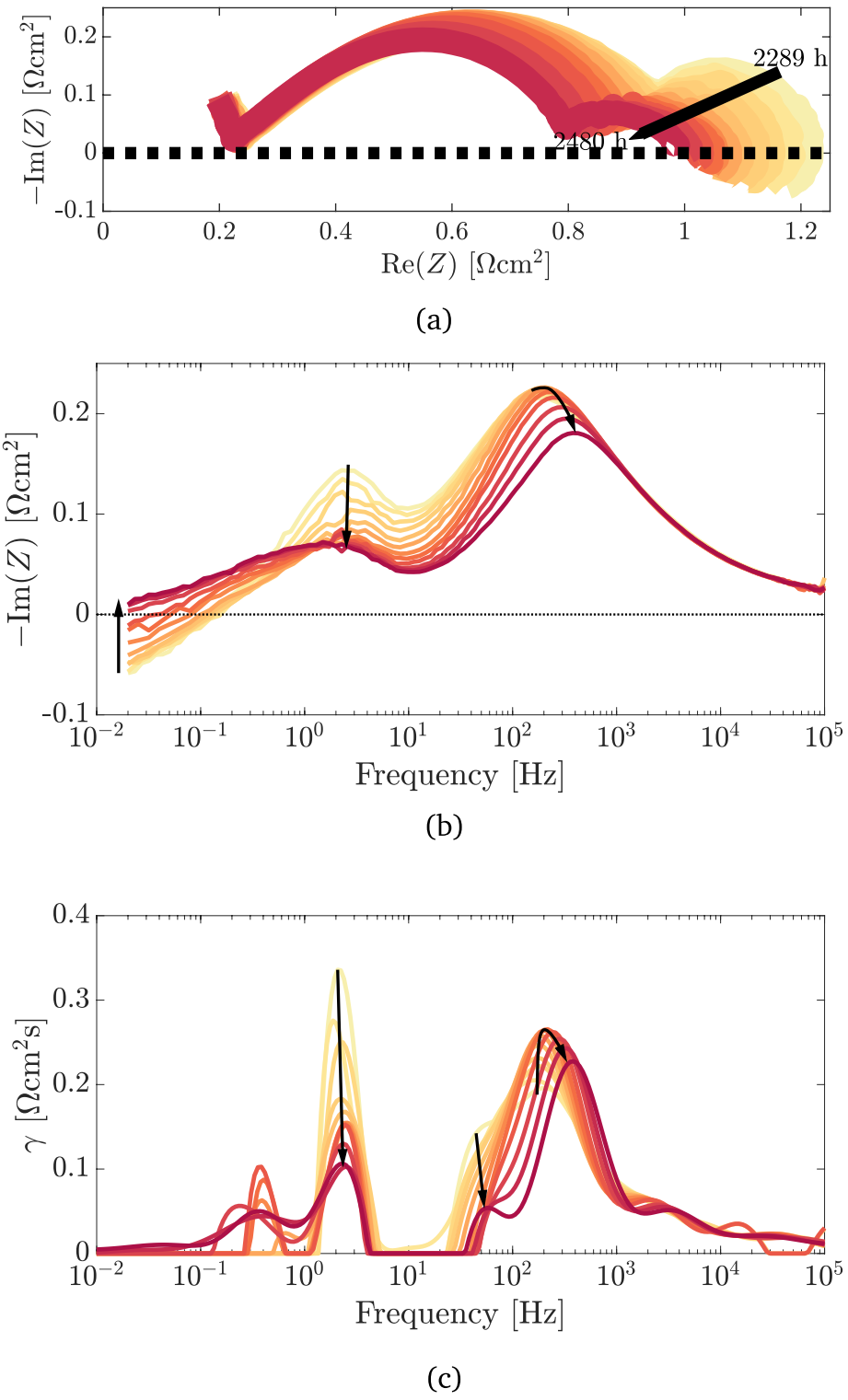

Figure 12. (a) and (b) electrochemical impedance spectra at 0.5 A cm^{-2} taken during the recovery following the exposure to 0.5 ppmv of SO_2 and (c) the corresponding DRT. Black arrows represent the observed trends of the time-evolution from the last measurement taken with 0.5 ppmv of SO_2 (2289 h) until the end of the recovery period (2480 h).

showed irreversible effects on the SOEC performances, especially in the high-frequency domain of the impedance spectra, indicating a permanent damage done to the electrochemically active nickel. The general contamination process was found to be similar to an SOFC exposed to H_2S: a fast initial degradation followed by a steady degradation rate. A good correlation was found between the surface coverage of nickel by sulphur and the relative increase in polarization resistance. Analysis of the DRT of the impedance measurements showed that the charge transfer and gas conversion peaks were particularly affected by the exposure to SO_2 confirming that the interaction between sulphur and the nickel present in the electrode reduces the electrochemical and catalytic reactions.

The OCV values were used to estimate the variation of the reactant composition due to the deactivation of the catalytic activity. The estimated amount of CO, calculated via thermodynamic equilibrium, was used as an indicator as CO originates only from the RWGS reaction. The estimated reduction in CO was only 7.5% when the SOEC was exposed to 5 ppmv of SO_2, corresponding to a nickel surface coverage of 0.93. This suggests a limited effect of the sulphur on the global catalytic activity under open circuit conditions. The reduction of the CO seemed to stabilize below 10%. In future works, gas chromatography, mass spectrometry, or another gas analysis methods could be used to assess the validity of these estimations.

The initial degradation rate was found to increase with the current density and the SO_2 concentration, the time needed to reach stabilization was found dependant on the SO_2 concentration and potentially to the current density, whereas no clear correlation was found for the height of the initial step and the final degradation rate. At a higher current density, the relative increase of the polarization resistance relative to the SO_2 content was found to be greater. This indicates that the current density has a negative impact on the SOEC tolerance to SO_2; however, further investigation is necessary to completely assess the effect of the current density.

The durability test performed at 0.5 A cm^{-2} showed a drastic increase of the cell voltage tens of hours after the beginning of the exposure leading to a voltage 'runaway' when the SOEC was exposed to 1 ppmv and 2 ppmv of SO_2. This behavior was characterized by a large increase of the serial resistance. When the SO_2 supply was cut, the serial resistance recovered almost entirely. The origin of this behavior is not clear yet but could be related to a cumulative effect of SO_2 leading to the total deactivation of the TPB close to the electrolyte, thus shifting the electrochemically active area further and virtually increasing the electrolyte thickness. The extent of the affected region close to the electrolyte was estimated to about 2 μm. This 'runaway' behavior was not observed during the exposure to 0.5 ppmv even after 500 h, suggesting that it is triggered by the SO_2 concentration and could be avoided by limiting the concentration to a sub-ppmv level in these operating conditions.

After successive exposure–recovery cycles, the SOEC's HE seemed weakened and a low frequency pseudo-inductive hook was observed. This low-frequency hook expanded when the SOEC was exposed to SO_2, disappeared during the recovery period, and seemed to be dependant on the cell exposure–recovery cycles history rather than on the SO_2 concentration. The origin of this low–frequency hook is not clear yet but could be related to the activation of an additional electrochemical reaction involving an intermediate species or electronic conductivity of the YSZ phase.

This work is expected to provide guidelines for future investigations on the interaction between sulphur and an SOEC's Ni-YSZ electrode. It will, also, help defining a threshold for future real power-to-X applications, especially regarding the required CO_2 quality.

Acknowledgments

The research leading to the presented work was funded by European Union's Horizon 2020 under grant agreement n° 699892 (ECo, topic H2020-JTI-FCH-2015-1). The anonymous reviewers are acknowledged for their valuable comments. Katelyn McClung is warmly thanked for the help she provided editing this publication.

Appendix A.

Figure A1 is a schematic representation of the SOEC voltage time evolution during poisoning by SO_2; values reported in table 2 are also represented and defined as follows:

t_i	Time at which SO_2 is introduced
t_s	Time at which the fast transient is passed
Δt	Time to stabilization
V_i	Initial or recovered SOEC voltage just before the SO_2 is introduced
V_s	SOEC voltage when t_s is reached
ΔV	Initial degradation step height
S_i	Initial degradation step rate
S_f	Final degradation rate

Appendix B.

A deeper discussion on the proposed mechanism explaining the reversible increase of R_s is presented in this appendix.

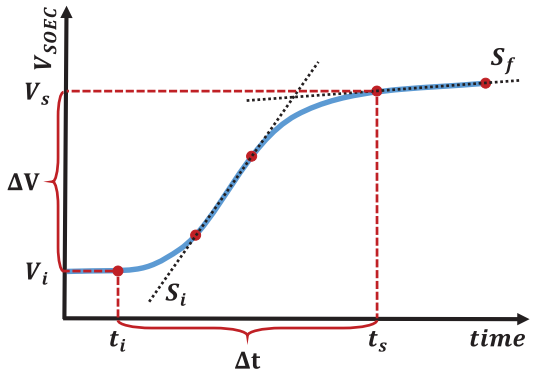

Figure A1. Schematic representation of the SOEC voltage time evolution during poisoning by SO_2.

Hypothesis 1 *A progressive reduction of the active area due to the deactivation by sulphur of the electrochemically active Ni from the higher (inlet) to lower (outlet) current density regions.*

As discussed in section 3.1, a higher current density may have a negative impact on the SOEC tolerance towards SO_2. Regions with a high current density could thus be deactivated first, leading to a reduction of the active area and a concomitant apparent increase of the area specific serial resistance. The current originally flowing through the now deactivated area would then be redistributed towards the cell outlet, locally increasing the current density. This increase in current density would trigger the deactivation process, gradually expanding the inactive regions from the SOEC inlet toward the outlet and leading to the observed voltage 'runaway' behavior. Assuming that a partial deactivation of the active area is analoguous to an electrode partial delamination, a concurrent and comparable increase of R_s and R_p is expected [42]. During the first voltage 'runaway' (from about 230 h to 500 h on figure 8), R_s and R_p increased by a factor of 2.1 and 1.1, respectively. A progressive deactivation of the active area is thus unlikely to be solely responsible for the observed behavior.

Hypothesis 2 *A cumulative effect of sulphur blocking the electrochemical active regions located closest to the electrolyte, possibly from the higher (inlet) to lower (outlet) current density regions.*

The electrochemically active region would be relocated away from the electrolyte, virtually increasing the electrolyte thickness. The serial resistance would automatically rise due to the increased distance that the oxygen ions have to travel to reach the OE and due to the constriction effect caused by the porosity of the HE compared with the dense electrolyte. The polarization resistance would not be greatly impacted, as the electrochemical reactions would not be affected, but only displaced. Once the SO_2 supply was cut, the blocked electrochemically active regions would be recovered, reducing the R_s. The virtual increase of the electrolyte thickness was evaluated considering the ratio (M) between the effective ionic conductivity of the YSZ phase present in the HE (σ_{eff}) and the bulk conductivity of YSZ (σ_0), which was estimated to about 0.15 from [48] assuming a volume fraction of YSZ $\varepsilon \approx 0.4$ [49]. The effective ionic conductivity of the porous electrode is [48]:

$$\sigma_{eff} = \sigma_0 \cdot M. \tag{B1}$$

The area specific resistance related to the virtual increase of the electrolyte thickness, L, becomes:

$$R_s^{virtual} = L \cdot \sigma_{eff}^{-1}, \tag{B2}$$

and the serial resistance:

$$R_s = R_s^{el} + R_s^{\text{virtual}} \tag{B3}$$

where $R_s^{el} = L^{el} \cdot \sigma_0^{-1}$ is the area specific resistance of the electrolyte, and L^{el} the electrolyte thickness. The contact resistance and electronic resistance in the electrodes are neglected. The thickness of the electrolyte being on the order of 10 μm, the extent of the deactivated region would be in the order of 2 μm, considering that R_s increased by a factor 2 to 3.

ORCID iD

G Jeanmonod https://orcid.org/0000-0003-2390-1138

References

[1] Hauch A, Jensen Søren H, Ramousse S and Mogensen M 2006 Performance and durability of solid oxide electrolysis cells *J. Electrochem. Soc.* **153** A1741–7
[2] Ebbesen S D and Mogensen M 2009 Electrolysis of carbon dioxide in solid oxide electrolysis cells *J. Power Sources* **193** 349–58
[3] Ebbesen S D, Graves C and Mogensen M 2009 Production of synthetic fuels by co-electrolysis of steam and carbon dioxide *Int. J. Green Energy* **6** 646–60
[4] Wang L, Pérez-Fortes M, Madi H, Diethelm S, herle J V and Maréchal Fçois 2018 Optimal design of solid-oxide electrolyzer based power-to-methane systems: A comprehensive comparison between steam electrolysis and co-electrolysis *Appl. Energy* **211** 1060–79
[5] Reiter G and Lindorfer J 2015 Evaluating CO_2 sources for power-to-gas applications—A case study for Austria *J. CO_2 Utilization* **10** 40–9
[6] Porter R T J, Fairweather M, Pourkashanian M and Woolley R M 2015 The range and level of impurities in CO_2 streams from different carbon capture sources *Int. J. Greenhouse Gas Control* **36** 161–74
[7] Porter R T J *et al* 2016 Techno-economic assessment of CO_2 quality effect on its storage and transport: CO_2 QUEST: An overview of aims, objectives and main findings *Int. J.Greenhouse Gas Control* **54** 662–81
[8] Wang J, Ryan D, Anthony E J, Wildgust N and Aiken T 2011 Effects of impurities on CO_2 transport, injection and storage *Energy Proc.* **4** 3071–8
[9] Madi H, Diethelm S, Ludwig C and Jan V H 2016 Organic-sulfur poisoning of solid oxide fuel cell operated on bio-syngas *Int. J. Hydrog. Energy* **41** 12231–41
[10] Sasaki K, Adachi S, Haga K, Uchikawa M, Yamamoto J, Iyoshi A, Chou J-T, Shiratori Y and Itoh K 2007 Fuel Impurity Tolerance of olid Oxide Fuel Cells *ECS Trans.* **7** 1675–83
[11] Haga K, Adachi S, Shiratori Y, Itoh K and Sasaki K 2008 Poisoning of SOFC anodes by various fuel impurities *Solid State Ion.* **179** 1427–31
[12] Matsuzaki Y and Yasuda I 2000 The poisoning effect of sulfur-containing impurity gas on a SOFC anode: Part I. Dependence on temperature, time and impurity concentration *Solid State Ion.* **132** 261–9
[13] Niakolas D K 2014 Sulfur poisoning of Ni-based anodes for Solid Oxide Fuel Cells in H/C-based fuels *Appl. Catalysis A: Gen.* **486** 123–42
[14] Sasaki K *et al* 2006 H_2S Poisoning of Solid Oxide Fuel Cells *J. Electrochem. Soc.* **153** A2023–9
[15] Zha S, Cheng Z and Liu M 2007 Sulfur Poisoning and Regeneration of Ni-Based Anodes in Solid Oxide Fuel Cells *J. Electrochem. Soc.* **154** B201–B206
[16] Kuhn J N, Lakshminarayanan N and Ozkan U S 2008 Effect of hydrogen sulfide on the catalytic activity of Ni-YSZ cermets *J. Mol. Catalysis A: Chem.* **282** 9–21
[17] Jablonski W S, Villano S M and Dean A M 2015 A comparison of H_2S, SO_2 and COS poisoning on Ni/YSZ and Ni/K2O-CaAl2O4 during methane steam and dry reforming *Appl. Catalysis A: Gen.* **502** 399–409
[18] Rasmussen J F B and Hagen A 2009 The effect of H_2S on the performance of Ni–YSZ anodes in solid oxide fuel cells *J. Power Sources* **191** 534–41
[19] Weber A, Dierickx S, Kromp A and Ivers-Tiffée E 2013 Sulfur Poisoning of Anode-Supported SOFCs under Reformate Operation *Fuel Cells* **13** 487–93
[20] Kromp A, Dierickx S, Leonide A, Weber A and Ivers-Tiffée E 2012 Electrochemical Analysis of Sulfur-Poisoning in Anode Supported SOFCs Fuelled with a Model Reformate *J. Electrochem. Soc.* **159** B597–B601
[21] Wang J-H and Liu M 2007 Computational study of sulfur–nickel interactions: A new S–Ni phase diagram *Electrochemistry Communications* **9** 2212–17
[22] Papurello D and Lanzini A 2018 SOFC single cells fed by biogas: Experimental tests with trace contaminants *Waste Manage.* **72** 306–12
[23] Papurello D, Lanzini A, Fiorilli S, Smeacetto F, Singh R and Santarelli M 2016 Sulfur poisoning in Ni-anode solid oxide fuel cells (SOFCs): Deactivation in single cells and a stack *Chem. Eng.* J. **283** 1224–33
[24] Hagen A 2013 Sulfur Poisoning of the Water Gas Shift Reaction on Anode Supported Solid Oxide Fuel Cells *J. Electrochem. Soc.* **160** F111–F118
[25] Kushi T 2017 Effects of sulfur poisoning on degradation phenomena in oxygen electrodes of solid oxide electrolysis cells and solid oxide fuel cells *Int. J. Hydrog. Energy* **42** 9396–405
[26] Zheng Y, Zhou J, Zhang L, Liu Q, Pan Z and Chan S H 2018 High-temperature electrolysis of simulated flue gas in solid oxide electrolysis cells *Electrochim. Acta* **280** 206–15
[27] Ebbesen S D, Graves C, Hauch A, Jensen Søren H and Mogensen M 2010 Poisoning of solid oxide electrolysis cells by impurities *J. Electrochem. Soc.* **157** B1419–29
[28] Wan T H, Saccoccio M, Chen C and Ciucci F 2015 Influence of the Discretization Methods on the Distribution of Relaxation Times Deconvolution: Implementing Radial Basis Functions with DRTtools *Electrochim. Acta* **184** 483–99
[29] Caliandro P, Nakajo A, Diethelm S and Van herle J 2019 Model-assisted identification of solid oxide cell elementary processes by electrochemical impedance spectroscopy measurements *J. Power Sources* **436** 226838
[30] Roine A 2015 HSC Chemistry® [Software] www.outotec.com/HSC
[31] He H P, Wood A, Steedman D and Tilleman M 2008 Sulphur tolerant shift reaction catalysts for nickel-based SOFC anode *Solid State Ion.* **179** 1478–82
[32] Hansen J Bøgild 2008 Correlating Sulfur Poisoning of SOFC Nickel Anodes by a Temkin Isotherm *Electrochem. Solid-State Lett.* **11** B178–80
[33] Cheng Z, Zha S and Liu M 2007 Influence of cell voltage and current on sulfur poisoning behavior of solid oxide fuel cells *J. Power Sources* **172** 688–93
[34] Brightman E, Ivey D G, Brett D J L and Brandon N P 2011 The effect of current density on H_2S-poisoning of nickel-based solid oxide fuel cell anodes *J. Power Sources* **196** 7182–7
[35] Hagen A, Johnson G B and Hjalmarsson P 2014 Electrochemical evaluation of sulfur poisoning in a methane-fuelled solid oxide fuel cell: Effect of current density and sulfur concentration *J. Power Sources* **272** 776–85
[36] Xia S J and Birss V I 2005 Deactivation and Recovery of Ni-YSZ Anode in H_2 Fuel Containing H_2S *ECS Proc. Vol.* **2005–07** 1275–83
[37] Yoshizumi T, Taniguchi S, Shiratori Y and Sasaki K 2012 Sulfur Poisoning of SOFCs: Voltage Oscillation and Ni Oxidation *J. Electrochem. Soc.* **159** F693–F701
[38] Barsoukov E and Ross Macdonald J 2005 *Impedance Spectroscopy: Theory, Experiment and Applications* (New York: Wiley) pp 13–20

[39] Leonide A 2010 SOFC modelling and parameter identification by means of impedance spectroscopy *PhD Thesis* Karlsruhe Institute of Technology, Germany
[40] Hagen A, Rasmussen J F B and Karl T 2011 Durability of solid oxide fuel cells using sulfur containing fuels *J. Power Sources* **196** 7271–6
[41] Hauch A, Hagen A, Hjelm J and Ramos T 2014 Sulfur poisoning of SOFC anodes: effect of overpotential on long-term degradation *J. Electrochem. Soc.* **161** F734–F743
[42] Gazzarri J I and Kesler O 2007 Non-destructive delamination detection in solid oxide fuel cells *J. Power Sources* **167** 430–41
[43] Vanhassel B, Boukamp B and Burggraaf A 1991 Electrode polarization at the Au, O_2(g)/yttria stabilized zirconia interface. Part I: theoretical considerations of reaction model *Solid State Ion.* **48** 139–54
[44] Pivac I and Barbir F 2016 Inductive phenomena at low frequencies in impedance spectra of proton exchange membrane fuel cells – A review *J. Power Sources* **326** 112–19
[45] Klotz D 2019 Negative capacitance or inductive loop? – A general assessment of a common low frequency impedance feature *Electrochem. Commun.* **98** 58–62
[46] Nechache A, Boukamp B A, Cassir M and Ringuedé A 2019a Premature degradation study of a cathode-supported solid oxide electrolysis cell *J. Solid State Electrochem.* **23** 109–23
[47] Nechache A, Boukamp B A, Cassir M and Ringuedé A 2019 Accelerated degradation of yttria stabilized zirconia electrolyte during high-temperature water electrolysis *J. Solid State Electrochem.* **23** 871–81
[48] Stenzel O, Pecho O, Holzer L, Neumann M and Schmidt V 2017 Big data for microstructure-property relationships: A case study of predicting effective conductivities *AIChE J.* **63** 4224–4232
[49] Rinaldi G, Nakajo A, Burdet P, Cantoni M, Chiu W K S and herle J V 2019 Characterization of Local Morphology and Availability of Triple-Phase Boundaries in Solid Oxide Cell Electrodes *Acta Mater.* **178** 194–206